Article

The Volume Stability of Alkali-Activated Electric Arc Furnace Ladle Slag Mortar and Its Performance at High Temperatures

Tung-Hsuan Lu [1], Ying-Liang Chen [2], Hong-Paul Wang [1],* and Juu-En Chang [1],*

1   Department of Environmental Engineering, National Cheng Kung University, No. 1, Daxue Rd. East Dist., Tainan City 701401, Taiwan; P58021029@ncku.edu.tw

2   Department of Resources Engineering, National Cheng Kung University, No. 1, Daxue Rd. East Dist., Tainan City 701401, Taiwan; roy.yl.chen@gmail.com

*   Correspondence: wanghp@mail.ncku.edu.tw (H.-P.W.); juuen@mail.ncku.edu.tw (J.-E.C.); Tel.: +886-6-2757575 (ext. 65850#32) (H.-P.W.); +886-6-2757575 (ext. 65824) (J.-E.C.); Fax: +886-6-2752790 (J.-E.C.)

Abstract: In this study, the engineering properties of Ordinary Portland Cement (OPC) and alkali-activated slag (AAS) mortar with electric arc furnace ladle slag (EAFLS) were investigated to reveal the effects of EAFLS on the expansion of cementitious mortars. Additionally, the effects of these two types of mortar were explored based on their compressive strength, especially at high temperatures. EAFLS in OPC mortars significantly reduced the compressive strength and caused serious soundness problems in the mortars after autoclaving due to the presence of free-CaO and free-MgO in the EAFLS slag. On the other hand, the AAS mortars produced with EAFLS had compressive strength comparable to ordinary OPC mortars and maintained soundness after autoclaving. During a 550 °C heat treatment, the OPC mortar cracked and lost residual strength, but the AAS mortar retained more than 90% of its residual strength. Even after an 800 °C heat treatment, the AAS mortar maintained 14% of its residual strength (about 4 MPa), sufficient to prevent the collapse of the specimen structure. The main reason is that alkali-activated technology can accelerate the hydration process and solve the delayed hydration problem. The results of this study indicated that EAFLS is suitable to partially replace the binder used in the production of AAS mortars, and the resulting AAS mortars have high volume stability, high compression strength, and good high temperature resistance.

Keywords: alkali-activated slag; electric arc furnace ladle slag; high temperature performance

1. Introduction

In recent years, researchers have attached great importance to the recycling of industrial byproducts and waste due to the raising consciousness of the need to achieve environmental sustainability [1,2]. Slag, the primary byproduct of steelmaking, is produced in a considerable amount, and the weathering of slag dump may cause potential environmental problems. For example, the amount of slag in Taiwan is 2.6 million tons per year, and it costs the government TWD (Taiwan New Dollars) 3 billion to treat. There are two ways to solve this issue, one is to decrease slag generation, and the other is to develop a reuse method [3].

Electric arc furnace ladle slag (EAFLS) has been used as civil engineering material such as road base layers and hot asphalt mixtures [4,5]. However, it cannot replace or be added into Portland cement due to its high content of free lime (free-CaO) [6–8]. Free-CaO and free-MgO may lead to volume expansion in a solid structure, and if the expansion stresses exceed the tensile strength of cement paste, cracks will occur [9]. This is a result of the hydration reactivity of free-CaO and free-MgO, which is slow and causes delays in expansion. Thus, the utilization of EAFLS is restricted, which means that solving the volume expansion problem is vital for slag recycling and reuse [10–15]. Previous research proposed specific weathering, curing treatment, and autoclave method to reduce volume

expansion of steel slag [16–18]. For example, open porosity is reduced after weathering and improving slag properties. The durability can also be strongly improved even in critical freezing/thawing environmental conditions by a small amount of air-entraining agent. However, the time for stabilizing furnace slag is related to the properties of the slag itself, so these methods may be time-consuming.

Alkaline activation materials (AAMs) are regarded as eco-friendly and sustainable alternatives to Portland cement [19]. AAMs are applied alkaline activators combined with pozzolanic materials that produce a solid material with properties comparable to traditional hydraulic cement [20]. AAMs have better chemical properties in terms of strength and, especially, high-temperature and fire resistance, as compared to Ordinary Portland Cement (OPC) systems [21–28]. Davidovits et al. reported that when immersed in 5% concentration hydrochloric and sulfuric acids for 4 weeks, alkali-activated binders displayed a mass loss of 6 to 7% in comparison with a mass loss of 78 to 95% for Portland-cement-based concretes [29]. Additionally, some articles showed that AAMs have good durability under different conditions [30–32] and can stabilize BOF (basic oxygen furnace) ladle slag [19]. Lee et al. mentioned that the study is to stabilize the BOF ladle slag by using geopolymer technology, as a vast quantity of free silicon can react with free-CaO and free-MgO to form stable silicate compounds resulting in the prevention of the expansion predicament [19].

EAFLS is mainly composed of calcium and silicon compounds, which could be a feasible raw material for AAMs. Moreover, reusing ladle slag can reduce the required cement amount, and this, in turn, reduces carbon emissions [33–35]. Hence, it is worth determining a method by which to solve the expansion problem and reuse EAFLS through the use of alkaline activation technology.

This study aims to use alkali-activated technology to improve soundness and enhance the activity of EAFLS. Furthermore, the engineering and environmental properties of alkali-activated ladle slag mortar were also investigated.

2. Materials and Methods

2.1. Materials

The EAFLS was sampled from a slag treatment plant in Taichung, Taiwan. Slag particles with a size smaller than 4.75 mm are too small to form aggregates, so another recycling method must be used. For particle sizes smaller than 0.15 mm, the proportion accounted for 28 % of the total EAFLS volume, as shown in Figure 1. However, according to ASTM C33/C33M-18 [36], the proportion of fine aggregates smaller than 0.15 mm should be less than 5% to meet the requirements of aggregate for use in concrete. In this research, all EAFLS was grounded small enough to pass through a 0.15 mm mesh and used to produce cementitious mortars (to produce LS in this research). Figure 2 shows the XRD patterns of the EAFLS, free-CaO, and free-MgO in the EAFLS, where it appears that using EAFLS as a concrete material may lead to volume instability.

Two cementitious mortars, ordinary Portland cement (OPC) mortar and alkali activated slag (AAS) mortar, were produced in this study by using OPC and ground-granulated blast-furnace slag (GGBFS) as binders, respectively. The OPC and GGBFS were replaced with 20 wt% of EAFLS (pass through a 0.15 mm mesh) for the mortar production. Samples were named OPC (OPC only), OPCLS (20 wt% of EAFLS and 80 wt% of OPC), AAS (GGBFS only), and AASLS (20 wt% of EAFLS and 80 wt% of GGBFS). Table 1 shows the chemical compositions of the EAFLS, where Ca, Si, and Mg were the main constituents. When using GGBFS as a binder, an aqueous solution that contains NaOH and Na_2SiO_3 was added as an alkaline activator. The alkali equivalent (Na_2O percentage by mass) was set at 4%, as stated in previous research [7], and the Ms. modulus (SiO_2/Na_2O molar ratio) was controlled to 1.25. The resulting cement mortars are typically called alkali-activated slag (AAS) mortars, and their mixing proportions are shown in Table 2. Moreover, the grain size of the cement particles in this study is within 7–200 μm (0.007–0.2 mm).
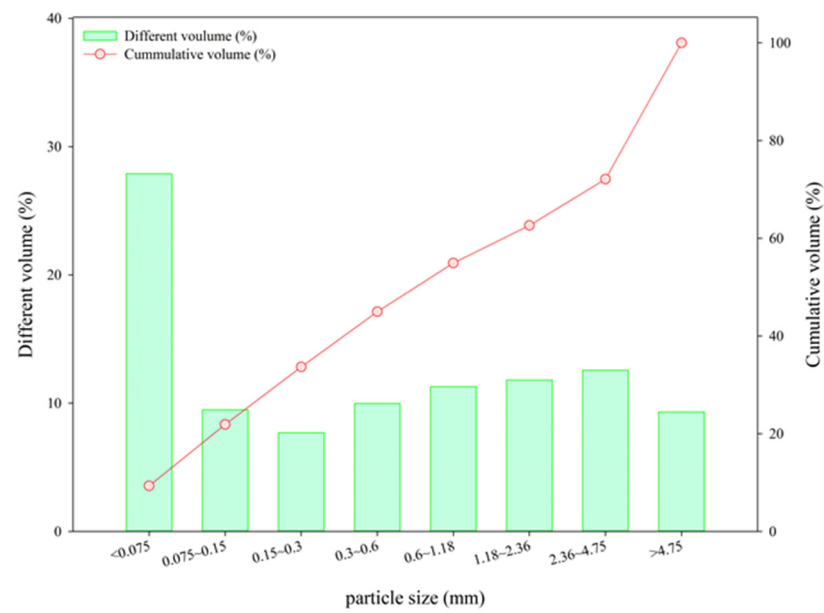
Figure 1. Particle size distribution of the electric arc furnace ladle slag (EAFLS).
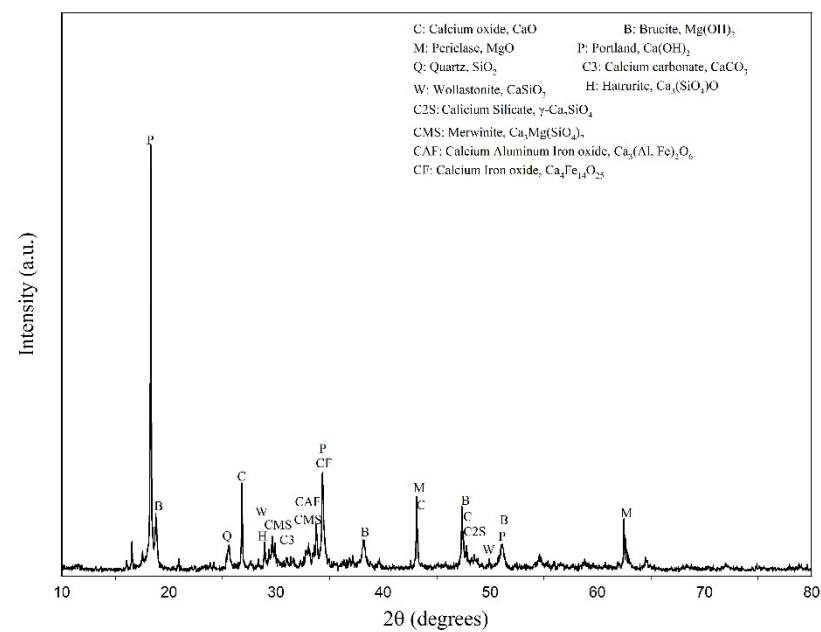

Figure 2. XRD patterns of EAFLS.

Table 1. Chemical composition of electric arc furnace ladle slag (EAFLS).

Chemical Composition		Electric Arc Furnace Ladle Slag
	Ca	29.25
	Si	4.77
Element (wt%)	Al	2.24
	Fe	2.83
	Mg	6.75

Table 2. Mixing proportions.

Specimen	W/B	OPC	Sand	GGBFS	EAFLS	Water	NaOH	Na$_2$SiO$_3$
OPC-paste	0.28	1000.0	-	-	-	280.0	-	-
OPCLS-paste	0.28	800.0	-	-	200.0	280.0	-	-
AAS-paste	0.28	-	-	1000.0	-	116.0	70.1	191.0
AASLS-paste	0.28	-	-	800.0	200.0	116.0	70.1	191.0
OPC-mortar	0.5	1000.0	2750.0	-	-	500.0	-	-
OPCLS-mortar	0.5	800.0	2750.0	-	200.0	500.0	-	-
AAS-mortar	0.5	-	2750.0	1000.0	-	336.0	70.1	191.0
AASLS-mortar	0.5	-	2750.0	800.0	200.0	336.0	70.1	191.0

-: No use; Concentration of NaOH$_{(aq)}$ is 45%; Concentration of Na$_2$SiO$_{3(aq)}$ is 34.3%.

According to the standard test methods ASTM C305-20 [37], ASTM C151/C151M [38], and ASTM C109/C109M [39], the mixing procedure is described below.

In the case of preparing paste (for testing autoclave expansion), first, cement and ladle slag and place the dry paddle in the mixing bowl. Then, add water and wait 30 s for the dry paddle to absorb the water. Turn on the mixer at a low speed (140 ± 5 r/min) for 30 s, then pause it for 15 s while scraping down into the batch any paste that may have collected on the sides of the bowl. Finally, switch on the mixer to medium speed (285 ± 10 r/min) for 60 s, fill the paste into bars mold (25 × 25 × 285 mm), and cure in a moist cabinet for 24 h. After that, the bars are removed from the molds and are ready for the autoclave expansion test. In the case of AAS paste, NaOH, Na$_2$SiO$_3$, and water are mixed before adding into the dry paddle.

In the case of preparing mortar (for testing compressive strength), as mentioned above, mix cement and ladle slag, and place the dry paddle in the mixing bowl afterward. Then, add water and turn on the mixer at a low speed (140 ± 5 r/min) for 30 s. Meanwhile, instead of pausing it, steadily pour in the entire quantity of sand within 30 s. Next, switch the mixer to a medium speed (285 ± 10 r/min) for 30 s, and pause it for 90 s to let the mortar stand. In the first 15 s, scrape down into the batch any mortar that may have collected on the sides of the bowl. After that, tighten up the mixer enclosure or cover the bowl with the lid. Finish by mixing for 60 s at a medium speed. The model is placed in the mortar cube mold (50 × 50 × 50 mm) and cured in a moist cabinet for 24 h. After 24 h, the cube is removed from the molds and stored in a saturated solution of calcium hydroxide until the curing time (3, 7, 28 days). In the case of AAS paste, NaOH, Na$_2$SiO$_3$, and water are mixed before adding into the dry paddle.

2.2. Material Testing and Analysis Methods

A thermogravimetric analyzer (DSC-TGA, TA Instrument, SDT 2960) was used to measure both the heat flows (DSC) and weight changes (TGA) of material in endothermic reactions over a wide temperature range. The samples were first homogenized and grounded into fine powders. Each grounded sample (40–50 mg) was loaded into an alumina crucible and was heated from ambient temperature to 1000 °C at a rate of 20 °C/min under air purging (100 mL/min). Figure 3 shows three endothermic reactions; the first was associated with the elimination of free water. The second and third endothermic effects attributed to the dihydroxylation of Ca(OH)$_2$ and Mg(OH)$_2$ were respectively in the temperature ranges from 380 to 420 °C and 440 to 520 °C. Under the autoclave condition, the Ca(OH)$_2$ and Mg(OH)$_2$ content in the paste sample could be derived from the weight loss of H$_2$O in the TGA curve by considering the following equations [40].

$$Ca(OH)_{2\,(s)} \rightarrow CaO_{\,(s)} + H_2O_{\,(g)} \tag{1}$$

$$Mg(OH)_{2\,(s)} \rightarrow MgO_{\,(s)} + H_2O_{\,(g)} \tag{2}$$
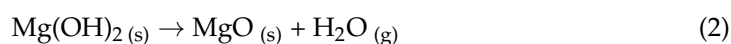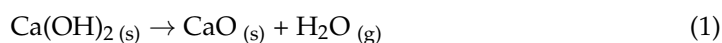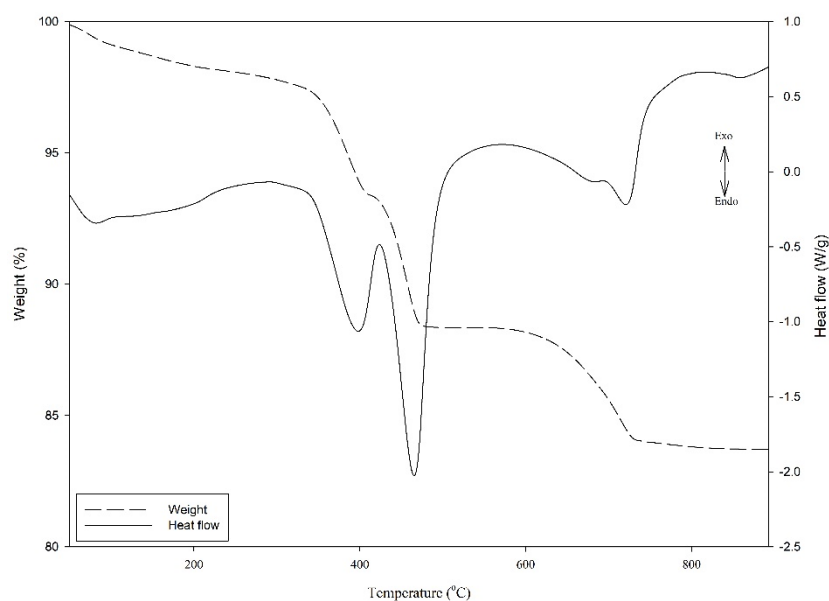
Figure 3. Illustration diagram of TGA result.

The free CaO content was determined by the chemical extraction method referring to ASTM C114-18 [41]. The extraction solution was prepared by mixing glycerin ($C_3H_8O_3$) with ethanol in a ratio of 1:2, and phenolphthalein ($C_{20}H_{14}O_4$) was selected as an indicator for the subsequent titration. In the extraction procedure, 60 mL of the glycerin–ethanol solution was transferred into a 250 mL boiling flask, in which 2 g of strontium nitrate ($Sr(NO_3)_2$) and 1 g of sample were added. The boiling flask containing the solution mixture was attached to a water-cooled condenser, being boiled continuously on a magnetic stirrer hot plate for 20 min. After the solution mixture was filtrated, the pink filtrate was boiled again and immediately titrated with standard ammonium acetate ($NH_4C_2H_3O_2$) solution (by dissolving 16 g of desiccated ammonium acetate in 1 L of ethanol, 1 mL = 0.005 g CaO) to a colorless endpoint.

In the mineralogical analysis, an X-ray diffractometer (Bruker, D8 Advance) was used to identify the mineral phases. The samples were homogenized, grounded to 75 μm (NO. 200 mesh, USA standard testing sieve), and pressed flat on a disc. All XRD analyses were carried out under the following parameters: (1) scanning range of 10–80° (2θ), (2) a step size of 0.05°, and (3) data acquisition rate of 2 s per step. The XRD analysis was performed on the raw material of EAFLS, sample conducted before and after the autoclave test, and sample conducted after the heating test.

The autoclave expansion test (ASTM C151/C151M [38]) was employed to determine the volume stability of EAFLS. The hardened paste specimens were molded with a size of 2.5 × 2.5 × 280 mm, being cured in a moist closet for 24 h, and were removed from the molds. The test procedure was carried out in an autoclave set at 2 ± 0.07 MPa pressure for 3 h, and the changes in the length of the specimen were calculated afterward.
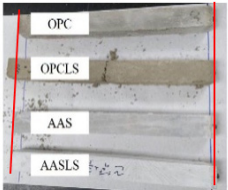
The OPC and AAS mortars were produced referring to the ASTM C109/C109M test method [39], and the 50 mm cubic specimens were prepared for compressive strength test. After curing in the moist closet for 24 h, the hardened mortar specimens were removed from the molds and placed into a saturated solution of calcium hydroxide until the curing time (3, 7, 28 days). To test high-temperature resistance capability, the 28-day cubic specimens were heated in a furnace for 3 h at a temperature of 200, 550, and 800 °C, respectively. Next, the specimens were removed from the furnace to cool down for a compressive strength test.

3. Results and Discussion

3.1. The Volume Stability of Alkali-Activated Electric Arc Furnace Ladle Slag Paste

Volume stability is crucial for concrete materials. However, previous studies pointed out the free-CaO or the free-MgO content in material would cause volume instability [42–45], and the same phenomenon was also observed in LS [46,47]. An autoclave expansion test referring to ASTM C151/C151M [38] was employed to determine the material stability (the length change of a cement paste should be smaller than 0.8%). Table 3 shows that the addition of EAFLS into OPC paste would lead to volume instability and cracking, which is similar to previous studies [42–45]; while using EAFLS with alkali-activated technology, the volume remains stable.

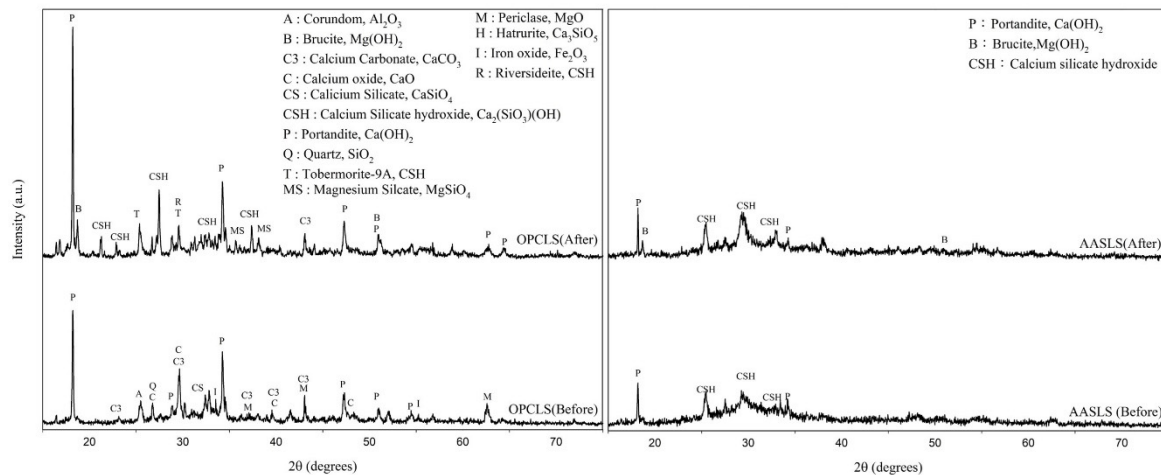**Table 3.** Effect of different hydration processes with EAFLS on volume stability.

Specimen	Length Change (%)	Soundness Expansion *	After the Autoclave Expansion Test
OPC	0.111	Stable	
OPC with 20% EAFLS (OPCLS)	Crack	Unstable	
Alkali-activated slag—control (AAS)	0.081	Stable	
AAS with 20% EAFLS (AASLS)	0.149	Stable	

*: Stable: length change <0.8; Unstable: length change >0.8.

The content of free-CaO and free-MgO in cement can react with moisture and transform into $Ca(OH)_2$ and $Mg(OH)_2$, causing volume increases [42,43]. In general, the reactivity of CaO and MgO is fast; that is, they turn into hydroxide before the paste becomes hard. However, due to the high-temperature processes in steelmaking, the free-CaO and free-MgO in ladle slag reach a dead-burnt status and exhibit lower reactivity. Low reactivity would lead to a hydration reaction of free-CaO and free-MgO after setting and thus cause volume instability [42,43,45,48]. Slags with free-CaO or free-MgO contents are suitable to use AAS technology to prevent volume instability since the silicon content in the alkali activator transforms free-CaO and free-MgO into CSH and MSH, respectively [7,19]. Additionally, Shi indicated that the ladle slag fines exhibit significant cementitious properties in the presence of an alkaline activator [11].

Alkali-activated technology can stabilize EAFLS by accelerating the hydration process [21–28,49]. Figure 4 on the left shows that the free-MgO in OPCLS paste could be all converted into $Mg(OH)_2$ after the autoclave expansion testing, proved by the signal of free-MgO and $Mg(OH)_2$ only present before and after the test, respectively. Moreover, after the autoclave expansion test, the intensity of the free-CaO decreased while the $Ca(OH)_2$ increased.

In AASLS paste, both the free-CaO and the free-MgO do not exist before the autoclave expansion test, meaning that the alkaline activator can accelerate the hydration process and transform free-CaO and free-MgO into $Mg(OH)_2$ and $Ca(OH)_2$. That is, without an alkaline activator, the free-CaO and free-MgO are still present in OPC paste after 24 h of curing in a moist closet. Table 4 presents the content of free-CaO by using chemical extraction [41]. Compared to the OPC type, little free-CaO content through the AAS process can be extracted. Moreover, after the autoclave expansion test, changes in the amount of $Ca(OH)_2$ and $Mg(OH)_2$ in OPCLS paste were 10.47% and 7.59%, respectively. By contrast, in the AAS paste, changes in the amount of $Ca(OH)_2$ and $Mg(OH)_2$ were relatively small, only 0.07% and 2%, respectively.

Figure 4. XRD patterns of different hydration processes with EAFLS before and after the autoclave expansion test (left) OPCLS (right) AASLS.

Table 4. Effects of different hydration processes on the changes in the amount of Ca(OH)$_2$ and Mg(OH)$_2$ before and after the autoclave expansion test and the amount of free-CaO before the autoclave expansion test.

Specimen	Ca(OH)$_2$ (%)		Mg(OH)$_2$ (%)		Free-CaO (%)
	Before	After	Before	After	Before
OPCLS	12.58	23.05	3.44	11.03	11.84
AASLS	4.22	4.29	2.67	4.67	0.84

3.2. Properties of Alkali-Activated Electric Arc Furnace Ladle Slag Mortar at High Temperatures

Table 5 provides the compressive strength of the OPC and AAS mortars produced with/without EAFLS in different curing periods. In the case without EAFLS, the compressive strength of the OPC mortars gradually increased from 22.3 to 32.1 MPa in a curing time of 3 to 28 days. As for AAS, the compressive strength gradually increased from 28.5 to 40.9 MPa. Both the OPC and AAS satisfied the standard compressive strength requirements for hydraulic cement Type GU (for general construction), which are 13.0 MPa on day 3, 20.0 MPa on day 7, and 28.0 MPa on day 28 (ASTM C1157/C1157M [50]). In the case of EAFLS, AASLS also met the above criteria and were even stronger than OPC on day 28. On the other hand, the compressive strength of OPCLS also increased continuously with curing time despite failing to meet the standard requirements outlined in ASTM C618 [51]. Table 5 also shows the relative compressive strength; when replacing OPC with 20 wt% LS, the compressive strength was significantly affected, probably due to the slow cementitious property of γ-Ca$_2$SiO$_4$ in water [6,11,52]. Therefore, a 20% EAFLS replacement decreased the compressive strength by 27% in OPC in 28 days. On the other hand, AASLS exhibited increasing compressive strength by up to 105% since AAS technology can accelerate the hydration process and in turn enhance the cementitious properties of EAFLS. Additionally, AASLS exhibited a high relative compressive strength (116%) at early ages (3 days) when compared to OPCLS (73%). This result shows that EAFLS is more suitable for application on AAS mortars.

Research has shown that alkaline activation helps with the formation of CSH gel [53–55], especially in calcium-rich environments [53]. Yip et al. indicated that CSH gel could bridge the gap between different hydrated phases and unreacted particles [53], thereby resulting in the observed increase in mechanical strength for these binders.

Table 5. Compressive strength using various hydration processes for different curing duration.

| Curing Time (Days)	Compressive Strength (MPa)				Relative Compressive Strength (%)		
	OPC	**OPCLS**	**AAS**	**AASLS**	**OPCLS**	**AAS**	**AASLS**
3	22.3	16.3	28.5	25.9	73.1	127.8	116.1
7	28.9	20.2	32.7	29.3	69.9	113.1	101.4
28	32.1	23.5	40.9	33.8	73.2	127.4	105.3

Fire is an Achilles heel in the case of concrete. Fire safety has been garnering additional attention in recent years. In the heating test, the new cube was heated in a high-temperature furnace in which the temperature was maintained for 3 h at 200, 550, and 800 °C, respectively. After cooling down, tests were conducted to evaluate how compressive strength varies with temperature. Table 6 shows that OPC and OPCLS samples cracked at 550 °C and 800 °C, respectively, while AAS and AASLS samples showed a good tendency of better performance in compressive strength during the heating process. Khoury [56] suggested that calcium hydroxide dehydration is a key to explaining why concrete cannot be used for high-temperature applications. Table 4 shows that the OPC hydration process produces more $Ca(OH)_2$ than the AAS hydration process. Therefore, samples made of OPC mortar cracked easily at the temperature at which $Ca(OH)_2$ started to dehydrate. A significant loss of strength in the OPC concrete specimen at 400 °C was attributed to the loss of crystal water, resulting in a reduction of $Ca(OH)_2$ content [57,58]. On the other hand, a similar performance was observed on the AAS and AASLS specimens at 800 °C as well as on the experiment result in Aydın and Baradan's study [59].

Table 6. Effects of different hydration processes on high-temperature resistance.

Specimen	Compressive Strength (MPa)			
	Normal	**200 °C**	**550 °C**	**800 °C**
OPC	32.1	35.6	Crack	Crack
OPCLS	21.8	23.1	Crack	Crack
AAS	40.9	46.5	40.4	3.2
AASLS	34.2	36.3	31.6	4.9

Figure 5 shows the XRD analysis results for specimens at various temperatures. The intensity of the $Ca(OH)_2$ peak in OPC and OPCLS decreased respectively at 550 °C and 800 °C, which were both attributed to $Ca(OH)_2$ decomposition at 350 °C. Other studies have shown similar results, supporting the finding that OPC does not have good resistance at high temperatures [24,60,61]. As for AAS and AASLS, there was no signal of $Ca(OH)_2$ detected, meaning that the $Ca(OH)_2$ decomposing problem will not be an issue and thus better high-temperature stability can be expected for further application. The reason why AAS and AASLS still have compression strength at 800 °C might be deduced from the presence of the åkermanite–gehlenite produced in alkali-activated systems, which can be found not only in this study, but in previous research, as well [22,62,63]. This mineral has high-temperature stability as well as good mechanical properties [22,64,65], showing that the use of alkali-activated technology can probably produce high-temperature resistance concretes, promising safer use in construction.
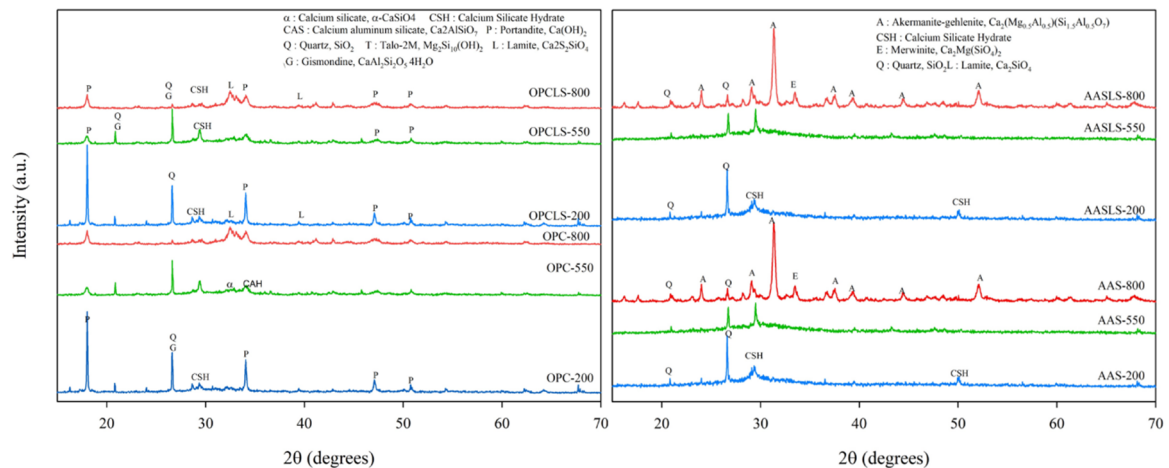
Figure 5. XRD patterns of OPC, OPCLS, AAS, and AASLS at various temperatures.

4. Conclusions

Based on the results of this research, the following conclusions can be drawn:

1. Using EAFLS in OPC mortar would cause volume instability due to the presence of free-CaO and free-MgO in the EAFLS slag. On the other hand, alkali-activated technology can accelerate the hydration process and resolve the delayed hydration problem. The length change of alkali-activated slag-control (AAS) and AAS with 20% EAFLS (AASLS) were only 0.081% and 0.149%, respectively. Therefore, EAFLS can become stable when used in an AAS mortar;

2. Adding EAFLS in the specific OPC mortar would decrease the compressive strength, resulting in failure to meet the criteria (ASTM C1157/C1157M). Alkali-activated technology could increase EAFLS cementitious properties for satisfying the criteria. For example, a 20% EAFLS replacement decreased the compressive strength by 27% in OPC in 28 days. On the other hand, AASLS exhibited increasing compressive strength by up to 105% since AAS technology can accelerate the hydration process and in turn enhance the cementitious properties of EAFLS.

3. Furthermore, alkali-activated technology also leads to good high-temperature resistance in cementitious materials. The compressive strength (MPa) of AAS and AASLS were 3.2 MPa and 4.9 MPa at 800 °C, respectively. It makes it possible to increase compressive strength by more than 5%, even at temperatures as high as 800 °C.

To summarize, there are difficulties associated with reusing EAFLS as a cementitious material in OPC mortar. However, using alkali-activated technology, EAFLS can be transferred into commonly used engineering material with excellent mechanical strength and fire resistance.

References

1. Nguyen, T.T.H.; Mai, H.H.; Phan, D.H.; Nguyen, D.L. Responses of concrete using steel slag as coarse aggregate replacement under splitting and flexure. *Sustainability* **2020**, *12*, 4913. [CrossRef]
2. Andrés-Vizán, S.M.; Villanueva-Balsera, J.M.; Álvarez-Cabal, J.V.; Martínez-Huerta, G.M. Classification of BOF slag by data mining techniques according to chemical composition. *Sustainability* **2020**, *12*, 3301. [CrossRef]
3. Du, C.; Gao, X.; Kitamura, S.Y. Measures to Decrease and Utilize Steelmaking Slag. *J. Sustain. Metall.* **2019**, *5*, 141–153. [CrossRef]
4. Brand, A.S.; Roesler, J.R. Steel furnace slag aggregate expansion and hardened concrete properties. *Cem. Concr. Compos.* **2015**, *60*, 1–9. [CrossRef]
5. González-Ortega, M.A.; Cavalaro, S.H.P.; Rodríguez de Sensale, G.; Aguado, A. Durability of concrete with electric arc furnace slag aggregate. *Constr. Build. Mater.* **2019**, *217*, 543–556. [CrossRef]
6. Shi, C.; Hu, S. Cementitious properties of ladle slag fines under autoclave curing conditions. *Cem. Concr. Res.* **2003**, *33*, 1851–1856. [CrossRef]
7. Lu, T.H.; Chen, Y.L.; Shih, P.H.; Chang, J.E. Use of basic oxygen furnace slag fines in the production of cementitious mortars and the effects on mortar expansion. *Constr. Build. Mater.* **2018**, *167*, 768–774. [CrossRef]
8. Emery, J.J. Slag utilization in pavement construction. In *Extending Aggregate Resources*; ASTM International: West Conshohocken, PA, USA, 1982.
9. Yildirim, I.Z.; Prezzi, M. Chemical, mineralogical, and morphological properties of steel slag. *Adv. Civ. Eng.* **2011**, *2011*, 463638. [CrossRef]
10. Das, B.; Prakash, S.; Reddy, P.S.R.; Misra, V.N. An overview of utilization of slag and sludge from steel industries. *Resour. Conserv. Recycl.* **2007**, *50*, 40–57. [CrossRef]
11. Shi, C. Characteristics and cementitious properties of ladle slag fines from steel production. *Cem. Concr. Res.* **2002**, *32*, 459–462. [CrossRef]
12. Tossavainen, M.; Engstrom, F.; Yang, Q.; Menad, N.; Larsson, M.L.; Bjorkman, B. Characteristics of steel slag under different cooling conditions. *Waste Manag.* **2007**, *27*, 1335–1344. [CrossRef] [PubMed]
13. Motz, H.; Geiseler, J. Products of steel slags an opportunity to save natural resources. *Waste Manag.* **2001**, *21*, 285–293. [CrossRef]
14. Geiseler, J. Use of steelworks slag in Europe. *Waste Manag.* **1996**, *16*, 59–63. [CrossRef]
15. Wu, S.; Xue, Y.; Ye, Q.; Chen, Y. Utilization of steel slag as aggregates for stone mastic asphalt (SMA) mixtures. *Build. Environ.* **2007**, *42*, 2580–2585. [CrossRef]
16. Santamaria, A.; Faleschini, F.; Giacomello, G.; Brunelli, K.; San José, J.-T.; Pellegrino, C.; Pasetto, M. Dimensional stability of electric arc furnace slag in civil engineering applications. *J. Clean. Prod.* **2018**, *205*, 599–609. [CrossRef]
17. Pellegrino, C.; Gaddo, V. Mechanical and durability characteristics of concrete containing EAF slag as aggregate. *Cem. Concr. Compos.* **2009**, *31*, 663–671. [CrossRef]
18. Wang, W.C. Feasibility of stabilizing expanding property of furnace slag by autoclave method. *Constr. Build. Mater.* **2014**, *68*, 552–557. [CrossRef]
19. Lee, W.H.; Cheng, T.W.; Lin, K.Y.; Lin, K.L.; Wu, C.C.; Tsai, C.T. Geopolymer technologies for stabilization of basic oxygen furnace slags and sustainable application as construction materials. *Sustainability* **2020**, *12*, 5002. [CrossRef]
20. Puertas, F.; Martínez-Ramírez, S.; Alonso, S.; Vázquez, T. Alkali-activated fly ash/slag cements. Strength behaviour and hydration products. *Cem. Concr. Res.* **2000**, *30*, 1625–1632. [CrossRef]
21. Guerrieri, M.; Sanjayan, J.G. Behavior of combined fly ash/slag-based geopolymers when exposed to high temperatures. *Fire Mater. Int. J.* **2010**, *34*, 163–175. [CrossRef]
22. Zuda, L.; Rovnaník, P.; Bayer, P.; Černý, R. Thermal properties of alkali-activated slag subjected to high temperatures. *J. Build. Phys.* **2007**, *30*, 337–350. [CrossRef]
23. Buchwald, A.; Hilbig, H.; Kaps, C. Alkali-activated metakaolin-slag blends—Performance and structure in dependence of their composition. *J. Mater. Sci.* **2007**, *42*, 3024–3032. [CrossRef]
24. Guerrieri, M.; Sanjayan, J.; Collins, F. Residual strength properties of sodium silicate alkali activated slag paste exposed to elevated temperatures. *Mater. Struct. Constr.* **2010**, *43*, 765–773. [CrossRef]
25. Mendes, A.; Sanjayan, J.; Collins, F. Phase transformations and mechanical strength of OPC/Slag pastes submitted to high temperatures. *Mater. Struct. Constr.* **2008**, *41*, 345–350. [CrossRef]
26. Natali Murri, A.; Rickard, W.D.A.; Bignozzi, M.C.; VanRiessen, A. High temperature behaviour of ambient cured alkali-activated materials based on ladle slag. *Cem. Concr. Res.* **2013**, *43*, 51–61. [CrossRef]
27. Juenger, M.C.G.; Winnefeld, F.; Provis, J.L.; Ideker, J.H. Advances in alternative cementitious binders. *Cem. Concr. Res.* **2011**, *41*, 1232–1243. [CrossRef]
28. Duxson, P.; Fernández-Jiménez, A.; Provis, J.L.; Lukey, G.C.; Palomo, A.; van Deventer, J.S.J. Geopolymer technology: The current state of the art. *J. Mater. Sci.* **2007**, *42*, 2917–2933. [CrossRef]
29. Davidovits, J.; Comrie, D.C.; Paterson, J.H.; Ritcey, D.J. Geopolymeric concretes for environmental protection. *Concr. Int.* **1990**, *12*, 30–40.
30. Pacheco-Torgal, F.; Abdollahnejad, Z.; Camões, A.F.; Jamshidi, M.; Ding, Y. Durability of alkali-activated binders: A clear advantage over Portland cement or an unproven issue? *Constr. Build. Mater.* **2012**, *30*, 400–405. [CrossRef]

31. Fernandez-Jimenez, A.; García-Lodeiro, I.; Palomo, A. Durability of alkali-activated fly ash cementitious materials. *J. Mater. Sci.* **2007**, *42*, 3055–3065. [CrossRef]

32. Bakharev, T.; Sanjayan, J.G.; Cheng, Y.B. Resistance of alkali-activated slag concrete to acid attack. *Cem. Concr. Res.* **2003**, *33*, 1607–1611. [CrossRef]

33. Faleschini, F.; Brunelli, K.; Zanini, M.A.; Dabalà, M.; Pellegrino, C. Electric Arc Furnace Slag as Coarse Recycled Aggregate for Concrete Production. *J. Sustain. Metall.* **2016**, *2*, 44–50. [CrossRef]

34. Almulhim, M.S.M.; Hunt, D.V.L.; Rogers, C.D.F. A resilience and environmentally sustainable assessment framework (RESAF) for domestic building materials in Saudi Arabia. *Sustainability* **2020**, *12*, 3092. [CrossRef]

35. Wang, W.; Noguchi, T. Alkali-silica reaction (ASR) in the alkali-activated cement (AAC) system: A state-of-the-art review. *Constr. Build. Mater.* **2020**, *252*, 119105. [CrossRef]

36. *ASTM.C33/C33M-18*; Standard Specification for Concrete Aggregates. ASTM International: West Conshohocken, PA, USA, 2018.

37. *ASTM.C305-20*; Standard Practice for Mechanical Mixing of Hydraulic Cement Pastes and Mortars of Plastic Consistency. ASTM International: West Conshohocken, PA, USA, 2020.

38. *ASTM.C151/C151M-18*; Standard Test Method for Autoclave Expansion of Hydraulic Cement. ASTM International: West Conshohocken, PA, USA, 2018.

39. *ASTM.C109/C109M-16a*; Standard Test Method for Compressive Strength of Hydraulic Cement Mortars (Using 2-in. or [50-mm] Cube Specimens). ASTM International: West Conshohocken, PA, USA, 2016.

40. Kneller, W.A.; Gupta, J.; Borkowski, M.L.; Dollimore, D. Determination of original free lime content of weathered iron and steel slags by thermogravimetric analysis. *Transp. Res. Rec.* **1994**, *1434*, 17–22.

41. *ASTM.C114-18*; Standard Test Methods for Chemical Analysis of Hydraulic Cement. ASTM International: West Conshohocken, PA, USA, 2018.

42. Chatterji, S. Mechanism of expansion of concrete due to the presence of dead-burnt CaO and MgO. *Cem. Concr. Res.* **1995**, *25*, 51–56. [CrossRef]

43. Min, D.; Dongwen, H.; Xianghui, L.; Mingshu, T. Mechanism of expansion in hardened cement pastes with hard-burnt lime. *Cem. Concr. Res.* **1996**, *26*, 647–648. [CrossRef]

44. Ali, M.M.; Mullick, A.K. Volume stabilisation of high MgO cement: Effect of curing conditions and fly ash addition. *Cem. Concr. Res.* **1998**, *28*, 1585–1594. [CrossRef]

45. Chatterji, S.; Jeffery, J.W. The volume expansion of hardened cement paste due to the presence of "dead-burnt" CaO. *Mag. Concr. Res.* **1966**, *18*, 65–68. [CrossRef]

46. Montenegro, J.M.; Celemín-Matachana, M.; Cañizal, J.; Setién, J. Ladle furnace slag in the construction of embankments: Expansive behavior. *J. Mater. Civ. Eng.* **2013**, *25*, 972–979. [CrossRef]

47. Suito, H.; Yokomaku, T.; Hayashida, Y.; Takahashi, Y. Effect of free lime on disintegration of LD slags. *Tetsu-To-Hagané* **1977**, *63*, 2316–2325. [CrossRef]

48. Mo, L.; Deng, M.; Tang, M. Effects of calcination condition on expansion property of MgO-type expansive agent used in cement-based materials. *Cem. Concr. Res.* **2010**, *40*, 437–446. [CrossRef]

49. Wang, S.-D.; Pu, X.-C.; Scrivener, K.L.; Pratt, P.L. Alkali-activated slag cement and concrete: A review of properties and problems. *Adv. Cem. Res.* **1995**, *7*, 93–102. [CrossRef]

50. *ASTM.C1157/C1157M-17*; Standard Performance Specification for Hydraulic Cement. ASTM International: West Conshohocken, PA, USA, 2017.

51. *ASTM.C618-19*; Standard Specification for Coal Fly Ash and Raw or Calcined Natural Pozzolan for Use in Concrete. ASTM International: West Conshohocken, PA, USA, 2019.

52. Kourounis, S.; Tsivilis, S.; Tsakiridis, P.E.; Papadimitriou, G.D.; Tsibouki, Z. Properties and hydration of blended cements with steelmaking slag. *Cem. Concr. Res.* **2007**, *37*, 815–822. [CrossRef]

53. Yip, C.K.; Lukey, G.C.; van Deventer, J.S.J. The coexistence of geopolymeric gel and calcium silicate hydrate at the early stage of alkaline activation. *Cem. Concr. Res.* **2005**, *35*, 1688–1697. [CrossRef]

54. Bignozzi, M.C.; Manzi, S.; Lancellotti, I.; Kamseu, E.; Barbieri, L.; Leonelli, C. Mix-design and characterization of alkali activated materials based on metakaolin and ladle slag. *Appl. Clay Sci.* **2013**, *73*, 78–85. [CrossRef]

55. Puertas, F.; Palacios, M.; Manzano, H.; Dolado, J.S.; Rico, A.; Rodríguez, J. A model for the C-A-S-H gel formed in alkali-activated slag cements. *J. Eur. Ceram. Soc.* **2011**, *31*, 2043–2056. [CrossRef]

56. Khoury, G.A. Compressive strength of concrete at high temperatures: A reassessment. *Mag. Concr. Res.* **1992**, *44*, 291–309. [CrossRef]

57. Georgali, B.; Tsakiridis, P.E. Microstructure of fire-damaged concrete. A case study. *Cem. Concr. Compos.* **2005**, *27*, 255–259. [CrossRef]

58. Handoo, S.K.; Agarwal, S.; Agarwal, S.K. Physicochemical, mineralogical, and morphological characteristics of concrete exposed to elevated temperatures. *Cem. Concr. Res.* **2002**, *32*, 1009–1018. [CrossRef]

59. Aydın, S.; Baradan, B. High Temperature Resistance of Alkali-Activated Slag-and Portland Cement-Based Reactive Powder Concrete. *ACI Mater. J.* **2012**, *109*, 463–470.

60. Saavedra, W.G.V.; de Gutiérrez, R.M. Performance of geopolymer concrete composed of fly ash after exposure to elevated temperatures. *Constr. Build. Mater.* **2017**, *154*, 229–235. [CrossRef]

61. Pan, Z.; Tao, Z.; Cao, Y.F.; Wuhrer, R.; Murphy, T. Compressive strength and microstructure of alkali-activated fly ash/slag binders at high temperature. *Cem. Concr. Compos.* **2018**, *86*, 9–18. [CrossRef]
62. Rovnaník, P.; Bayer, P.; Rovnaníková, P. Characterization of alkali activated slag paste after exposure to high temperatures. *Constr. Build. Mater.* **2013**, *47*, 1479–1487. [CrossRef]
63. Rashad, A.M.; Sadek, D.M.; Hassan, H.A. An investigation on blast-furnace stag as fine aggregate in alkali-activated slag mortars subjected to elevated temperatures. *J. Clean. Prod.* **2016**, *112*, 1086–1096. [CrossRef]
64. Zuda, L.; Rovnaník, P.; Bayer, P.; Černý, R. Effect of high temperatures on the properties of alkali activated aluminosilicate with electrical porcelain filler. *Int. J. Thermophys.* **2008**, *29*, 693–705. [CrossRef]
65. Zuda, L.; Pavlík, Z.; Rovnaníková, P.; Bayer, P.; Černý, R. Properties of Alkali Activated Aluminosilicate Material after Thermal Load. *Int. J. Thermophys.* **2006**, *27*, 1250–1263. [CrossRef]